INT 199/00 juillet 2000

ANALYSIS OF IMPURITY TRANSPORT IN TCV OHMIC DISCHARGES

A. Zabolotski, H. Weisen

Analysis of Impurity Transport in TCV Ohmic Discharges

A. Zabolostky, H. Weisen

Centre de Recherches en Physique des Plasmas
Association EURATOM-Confédération Suisse
École Polytechnique Fédérale de Lausanne
CH-1015 LAUSANNE, Switzerland

Astract:

The transport of small amounts of aluminium injected into Ohmically heated plasma in the TCV tokamak is studied. A computer model, based on the STRAHL code, is used for modelling the experimental results. The radial flux density is described as a sum of diffusive and convective terms whose radial and temporal dependences are obtained by comparison of the experimental and the simulated data.

The radial dependences of transport parameters were obtained for $\rho_{pol}<0.5$ for the quiescent phases between consecutive sawtooth crashes and for the duration of the sawtooth crashes. The results show a temporal discontinuity of the transport parameters. The diffusion coefficient during the quiescent phase is of the order of 0.1 m^2/s at the centre of the plasma and rises to near 2 m^2/s at $\rho_{pol}\approx0.5$. The drift velocity is always directed inwards and rises from 0.05 m/s at the centre up to 5 m/s at $\rho_{pol}\approx0.5$. During the sawtooth crash, which lasts about 300 μs, the one-dimensional transport model roughly consists with experimental observations if the central diffusion coefficient is assumed to increase by more than an order of magnitude.

Introduction

The traces of injected impurities for present analysis were obtained using two different kinds of impurity sources. The first is laser oblation of impurity when high-power laser irradiation of aluminised slide produces a 5 ms burst containing about $5 \cdot 10^{18}$ neutral aluminium atoms. The second kind of impurity source is a small peace of aluminium oxide from plasma surrounding walls, which falls into plasma with low speed (so called UFO). This uncontrolled injection is observed in about 100 from 3000 shots and in about 30 shots soft x-ray radiation followed by injection changes by a factor of 6 while the changes of plasma parameters are not significant. The results are mainly based on UFO traces because the changes in soft X-ray radiation followed laser ablation were not sufficiently large to be analysed by described method. It is evident that UFO injection cannot be used for systematic analysis and are convenient for the first estimations only.

The time history and spatial distribution of injected impurity emission were followed as a function of time with X-ray tomography system comprising 200 viewing lines in 10 cameras with time resolution about 10 kHz. The 47 μm Be filter was used to cut off the light impurities line radiation (with the photon energy less than 1 keV). The tomographic inversion of the data was obtained using the Minimum Fisher Regularization method on a pixel grid with 38 mm of spatial resolution. Because of the Be filter the inversion gives reliable local emission in the plasma regions where electron temperature is higher then about 200 eV. Thomson scattering system of Nd lasers was used to measure the profile of electron density and electron temperature along the vertical chord. Spatial resolution of this system is about 35 mm and the time resolution is about 16 ms. The bolometer system based on fast AXUV diodes with temporal resolution less than 0.5 ms was used to obtain the form of the impurity source function. No spectroscopic measurements are available for these experiments.

Injection time histories and spatial profile

The following discussion refers in generally to shot No 16051, which has the typical parameters of so called standard TCV shot. The signals of the plasma current, line integrated electron density, electron temperature and the signal of one of the central chord of soft X-ray system in the case of UFO injection are depicted in figure 1. The injection of the impurity for this shot was made at time 1.0628 s into the Ohmic heated L-mode plasma with I_p=280 kA,

line-integrated electron density $n_e \approx 3 \cdot 10^{19}$ m^{-2} and central temperature $T_e \approx$ 800 eV. The sudden rise of the soft x-ray radiation (SXR) signal after injection time corresponds to the radiation from injected impurity.

It can be easily seen from figure 1 that during injection there are no significant disturbances of plasma parameters such as plasma current or electron density, while the integrated signal of soft X-ray radiation (SXR) rises about 16 times with respect to the background. The changes of the plasma current and linear density are less than 1%. The changes of the Z_{eff} are less than 10% at the centre. The precise changes of the electron temperature that follow the injection can't be deduced from present Thomson scattering measurements because the temperature have fluctuations faster than the temporal resolution.

The time history of the signal SXR radiation (fig. 2) is characterized by rapid increase after the injection, followed by a more gradual decay. As the impurity propagates inwards, it enters region of high electron density and high electron temperature, and the intensity of signal grows. After about 15 milliseconds the signal has a maximum and then starts to decay as the impurity continuously diffuses out. After about 60 ms the SXR reaches the previous background values. Sudden changes of the SXR signal, which can be more clearly observed at this signal during depletion phase, correspond to the sawtooth crashes.

The fall of the signal of SXR is well described by an exponential and yields a decay time of about 20 ms. That time can be interpreted as the global particle confinement time. The detail analysis based on this characteristic of the SXR signal was not performed because of lack of statistic.

At the figure 3 the tomographic reconstruction of the SXR emissivity distribution is shown versus the vertical coordinate at the major radius 0.9 m (Thomson chord). The background radiation was not subtracted.

During the quiescent phase of the first and second sawtooth an increasingly hollow emission distribution develops. Very slow evolution of this distribution at the centre shows that diffusion coefficient is very low over the central region, all the time except the sawtooth collapses. During the sawtooth crash, which lasts about 200-300 μs a significant redistribution of the impurities takes place. This causes a sudden rise of the signal at the central region and a flattening of the impurity density profiles at the core of the plasma. As it will be shown later such redistribution during the ingress phase can't be explained only by temperature changes and modifications of the diffusion coefficient and drift velocity are

needed. At first two crashes the SXR shows inverted sawtooth behaviour. After about three crashes the impurity finally fills the central region creating the peaking profile of emission, which is flattened at the core by every crash, displaying the normal sawtooth behaviour when the impurity ions displace outwards. During this phase, when the peaking profile of impurity has already developed the influence of the inward drift can be clearly observed.

The transport code STRAHL

Code STRAHL was used as the main tool for obtaining transport parameters. STRAHL is an interactive, stand-alone, 1D impurity transport code, which has been used since 1980 on several devices. It calculates the impurity ionisation balance on the basis of given plasma parameters and empirical transport models.

The code calculates the solution of the equation of impurity particle conservation for each ionisation stage

$$\frac{\partial n_{I,Z}}{\partial t} = -\nabla\vec{\Gamma}_{I,Z} + Q_{I,Z}$$

where $\Gamma_{I,Z}$ is the flux density of the impurity and $Q_{I,Z}$ is the source/sink term, which includes ionisation, radiative, dielectronic and charge exchange recombination from and to the neighbouring ionisation stages.

The impurity flux density is represented as the sum of two terms:

$$\Gamma_Z(r) = -D(r)\frac{\partial n_Z}{\partial r} + v(r)n_Z(r),$$

where the gradient term represents self-diffusion, while the other, the convective term, is due to gradients in ion temperature and in the other impurity densities.

After the transformation including the integration over the volume inside a flux surface and introducing volume flux surface label $\rho_{vol} = \sqrt{\frac{V}{2\pi^2 R_{axis}}}$ the initial equation can be rewritten on the form

$$\frac{\partial n_{Z,I}}{\partial t} = \frac{1}{\rho_{vol}}\frac{\partial}{\partial \rho_{vol}}\rho_{vol}\left(D^*\frac{\partial n_{Z,I}}{\partial \rho_{vol}} - v^* n_{Z,I}\right) + Q_{Z,I}$$

where $D^* = < D_{\rho\rho} |\nabla\rho|^2 >$, $v^* = < v_\rho |\nabla\rho| >$ and <...> means flux surface average. D^* and v^* have an anomalous and a neo-classical parts.

Background plasma parameters

To make a simulation of impurity behaviour using STRAHL code the background plasma parameters such as electron temperature, electron density, geometry as well as source function are needed.

The plasma geometry inside the last closed flux surface (LCFS), which is assumed to be independent of time, can be taken from equilibrium reconstruction. Temperature and density data are taken from Thomson scattering system. As was mentioned above the temporal resolution of Thomson scattering system used on TCV is about 15 ms. Such resolution is not sufficient to describe the temperature changes during injection event. As an example, at figure 2, the bold points show the times where the temperature and density measurements are available. In this case, valuable information about temperature time dependence can be obtained in quasi-stationary cases where repetitive measurements at lower frequency produce samples at different phases of cycle. It is clear that this approach cannot take into account neither fluctuations during sawtooth cycles nor the changes of the temperature following the injection.

The electron density profile was taken constant for all injection time because of the fact that discontinuous jumps during the crash for n_e are much smaller than for T_e. Examples of sampling procedure are shown at figure 4.

The form of source function can be obtained using the signal of the edge chord of fast bolometer system based on AXUV diodes (see figure 5). The signal, presented at figure 6 was chosen as source function in the case of UFO injection. The quantity of the particles, which penetrate into the plasma (i.e. the normalization of the integral of the source function over the time), remains undefined and up to now it seems that there is no way to determine this parameter from the available experimental data. Simulation was made using wide range of normalization and discussion of the influence of this parameter on results will be presented in the next section.

Determination of transport parameters

As was mentioned above, the ingress phase of the signal is more favourable for determination of diffusion coefficient since during this phase the gradient of the impurity density is quite high and the diffusion term is dominate.

The radial transport equation was solved for each phase of signal (sawteeth crash or quiescent phase) separately. The final distribution of the impurity density of one phase of signal was used as an initial condition for the following one. The crucial problem of such approach is the accumulation of the errors in the impurity density distribution from each simulation phase and, as a consequence, difficulties in simulations of the later phases of the signal. In practice, to determine the transport parameters up to three first sawtooth cycles were used

For the extraction of the diffusion coefficient and drift velocity, discrete points interpolation of D along the radius were used. In each point the values of D were independently changed in order to reproduce the absolute values and the time behaviour of ΔSXR profiles. The drift velocity was adjusted automatically by STRAHL in such a way that the final impurity concentration in the source free region at steady state was constant. Profiles of the diffusion coefficient and the drift velocity were kept constant in time throughout in the simulation of one particular phase of the signal (quiescent phase or sawtooth crash) that can be justified by a shot duration of the analysed phenomena.

The experimental profiles of ΔSXR emission for comparison with the simulated ones were obtained by subtraction of time dependent background assuming that emission of background plasma modulated by sawtooth persists during all injection phase (figure 7). Usage of the first quiescent phase just after the start of injection for deriving central transport parameters is rather delicate procedure because of the uncertainties in the background subtraction. This problem can arise also for second and even for the third sawtooth cycle if the changes of SXR following the injection are not significant (in general, ΔSXR <10 in the maximum of the signal).

The oscillations of emission just after sawtooth crash make it necessary to choose only those values of the diffusion coefficient that fit best the second half of the phase. During the first half the difference about 20 % in absolute value between simulated and experimental profiles was considered as tolerant.

Underestimation of the gradient in experimental profiles of SXR due to limited spatial resolution of the soft x-ray system was not taken into account during the fitting procedure.

To obtain the transport parameters the normalisation of source function was being varied from $1 \cdot 10^{17}$ up to $5 \cdot 10^{18}$ particles in total. The values outside this range lead to the problems in the fitting procedure. In particular, the values of normalisation that are lower than $1 \cdot 10^{17}$ particles in total demand to reduce the diffusion coefficient down to 0 at $\rho_{pol}=1$ while the

values of D at $\rho_{pol} \approx 0.8$ rise to values 5 m^2/s. For values higher than $5 \cdot 10^{18}$ particles, the rise of the simulating emission during the first quiescent phase just after the injection is much faster then the experimental one.

On figures 9 and 10 the experimental profiles of ΔSXR (thin solid lines) for different values of normalisation during the quiescent phases are shown in comparison with the simulated ones (dashed and thick solid lines). The resulting radial dependencies of D and V for different values of the source function normalisation are shown at the figures below.

The figure 13 presents the influence of the uncertainties in the temperature on the simulated profiles of ΔSXR at the particular time moment. The filled area corresponds to the errors of ±5 % in absolute values of the temperature. The corresponding changes of the diffusion coefficient are also shown. Such errors of the temperature lead to uncertainties in diffusion coefficient of about 50% at the centre and more than 100 % at the edge.

The variation of the transport parameters from one quiescent phase to another during the one shot is not significant for $\rho_{pol} < 0.5$. The variations for outer region are smaller than the uncertainties due to undefined source function.

The changes of the temperature during sawtooth crash at the ingress phase lead to the changes of SXR of only about 10% and cannot explain the flattening of the ΔSXR profiles shown on figure 3. To simulate those flattening the diffusion coefficient was increased by an order of magnitude for the time period lasting about 300-400 μs. On figure 14 the experimental profiles of ΔSXR (dashed lines) during the sawtooth crash are shown in comparison with the simulated ones (solid lines). The diffusion coefficient and drift velocity that fit best the experimental profiles, are shown below. Since the duration of the sawtooth crash is relatively short the values of the D and V outside $\rho_{pol}=0.5$ region have no influence on transport at the centre and rest undefined. It results in the fact that the source function does not play role in determination of the transport parameters during the sawtooth crashes. The errors in D and V appear due to undefined duration of the crash and oscillations of the emission just before and after the crash. That leads to uncertainties in choosing of start and final emission profiles.

Summary and conclusions

From the previous analysis it can be concluded that due to numerous uncertainties, the transport parameters outside $\rho_{pol}=0.5$ rest undefined and will be omitted from now on. On the

figure 16 the resulting diffusion coefficient and drift velocity for central plasma region during quiescent phases, are shown. The dashed line indicates the location of q=1 surface. The presented values of the D are accurate within about 50 %, which is indicated by filled area. Rise of the diffusion coefficient from the core to the edge up to the values of ρ_{pol}=0.5 can be roughly interpolated for this shot by exponential function $D(r) = D_0 \exp(r/\lambda)$ with D_0= 0.08 m^2/s and λ= 4±0.7 cm. The drift velocity (figure 17) is always directed inwards with low values at the centre and with nearly linear rising up to –1.5 m/s at the ρ_{pol}≈0.5. This behaviour cannot be extrapolated at the outer regions because as it is indicated on figures 9 and 10 the very high inward drift is observed there. It should be mentioned that such high values of the drift velocity at the edge of the plasma are observed for all range of the normalisations used. The same results for the diffusion coefficient were obtained for the shots No. 16754 and No 16079 (figure 20 and 22) with the identical background plasma parameters. However in the case of shot 16754 (figure 22) the exponential approximation rises faster than real D. In the case of shots No. 16754 and No 16079 (figure 21 and 23) the rise of drift velocity in the core is more complicated than linear approximation because the transition region from the low to high drift is closer to the centre.

Relatively low values of the diffusion coefficient at the centre and a rise to the edge are in good agreement with the results obtained on other tokamaks [4][5]. In spite of the fact that D can be lower than 0.05 m^2/s at the centre, this value remains larger than the one, obtained from neoclassical calculations, which in general is of the order of 10^{-3} m^2/s.

The present analysis shows that the sawtooth crashes lead to a strong increase of the central transport (figure 18). The diffusion coefficient increases by more than an order of magnitude while the drift velocity increases by a factor of 5.

It should be noted that the transport parameters during sawtooth crash were obtained in the model of one-dimensional transport and can serve only as an indication of discontinuity of the transport parameters. The existence of the more complicated two-dimensional flows that could be responsible for the particles exchange was shown in Ref [10].

The influence of the sawtooth activity on the central transport can be more clearly observed from the example at figure 28 which represents injection of Al by laser oblation into plasma with relatively low central density $1.9 \cdot 10^{19}$ m^{-3}, central electron temperature about 1000 eV and a rather short sawtooth period (≈1 ms). It is seen that reconstructed profile of the emission is never hollow that indicates that the central transport parameters are elevated.

Because of short sawtooth period, the analysis based on time average over sawtooth period was used. The resulting diffusion coefficient is shown on figure 29.

Acknowledgments

The authors would like to thank R.Dux for providing the STRAHL code.

References

[1] E.S. Marmar, at al., Nuclear Fusion, Vol. 22,No 12 (1982) p. 1567.

[2] K.H. Benringer, et al., Nuclear Fusion, Vol.26, No 6 (1986) p. 751.

[3] W.K. Leung, et al., Plasma Physics and Controlled Fusion. Vol. 28, No 12A, p. 1753.

[4] R. Dux, at al., Nuclear Fusion, Vol. 39, No 11 (1999), p. 1509.

[5] R. Giannella, et al., Nuclear Fusion, Vol. 34, No 9 (1994), p. 1185

[6] K.H. Burrel et al., Nuclear Fusion, Vol. 21, No 8 (1981), p. 1009.

[7] S.A. Cohen, at al., Physical Review Letters, Vol. 35, No 22 (1975) p.1507.

[8] H. Weisen, et al., Rev. Sci. Instrum. 62(6) (1991), p. 1531.

[9] R.Dux. STRAHL User Manual

[10] I.Furno et al., submitted for publication in Nuclear Fusion

[11] D.Pasini et al, Nuclear Fusion, Vol.30, No.10, (1990) p.2049

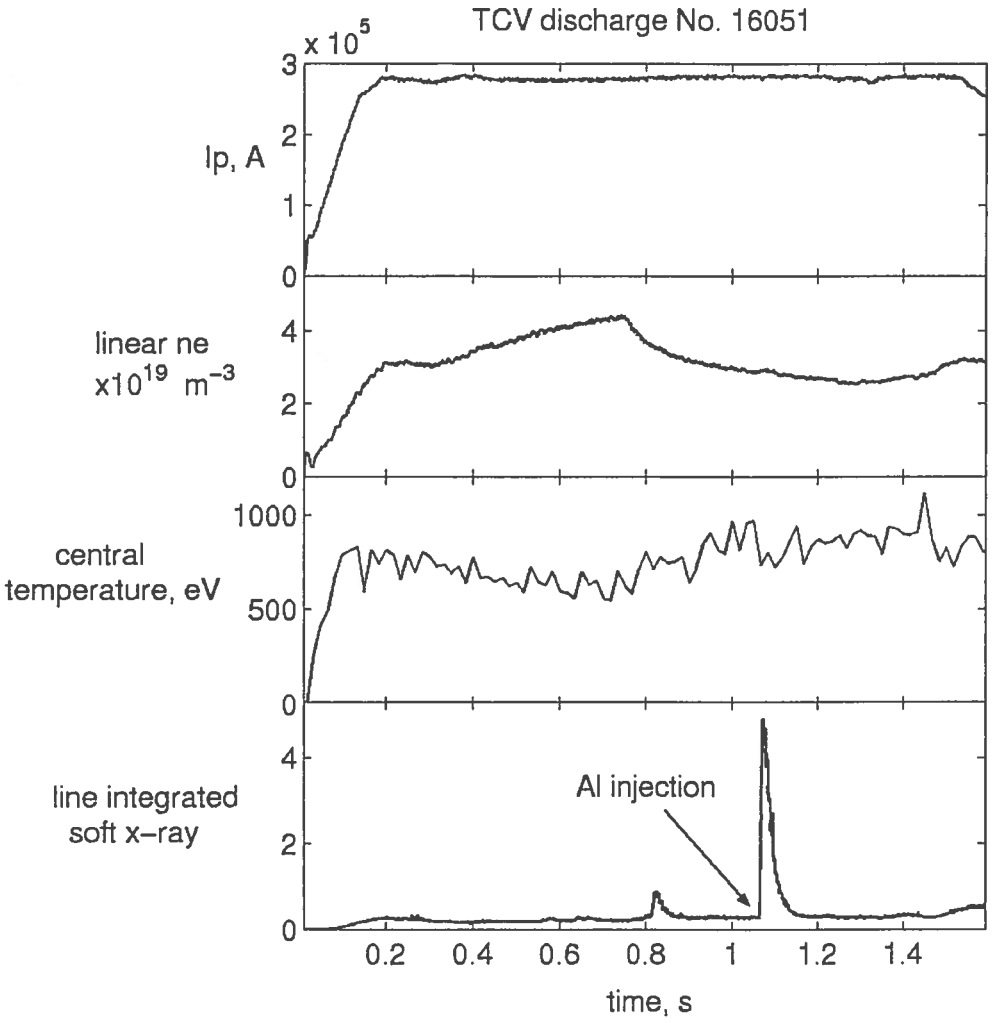

Figure 1 Time evolution of plasma current, linear density, central temperature and line integrated soft x-ray intensity

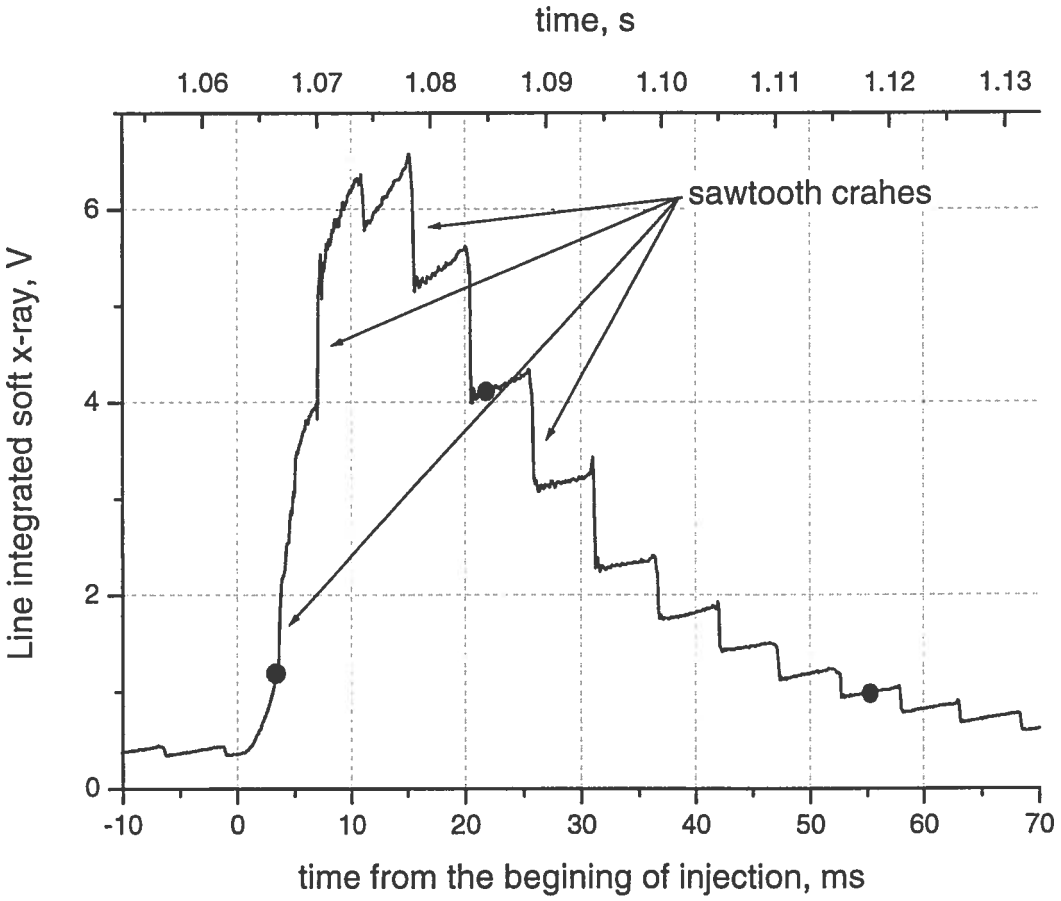

Figure 2 Time evolution of line integrated soft x-ray intensity. Black points show where the Thomson data exist.

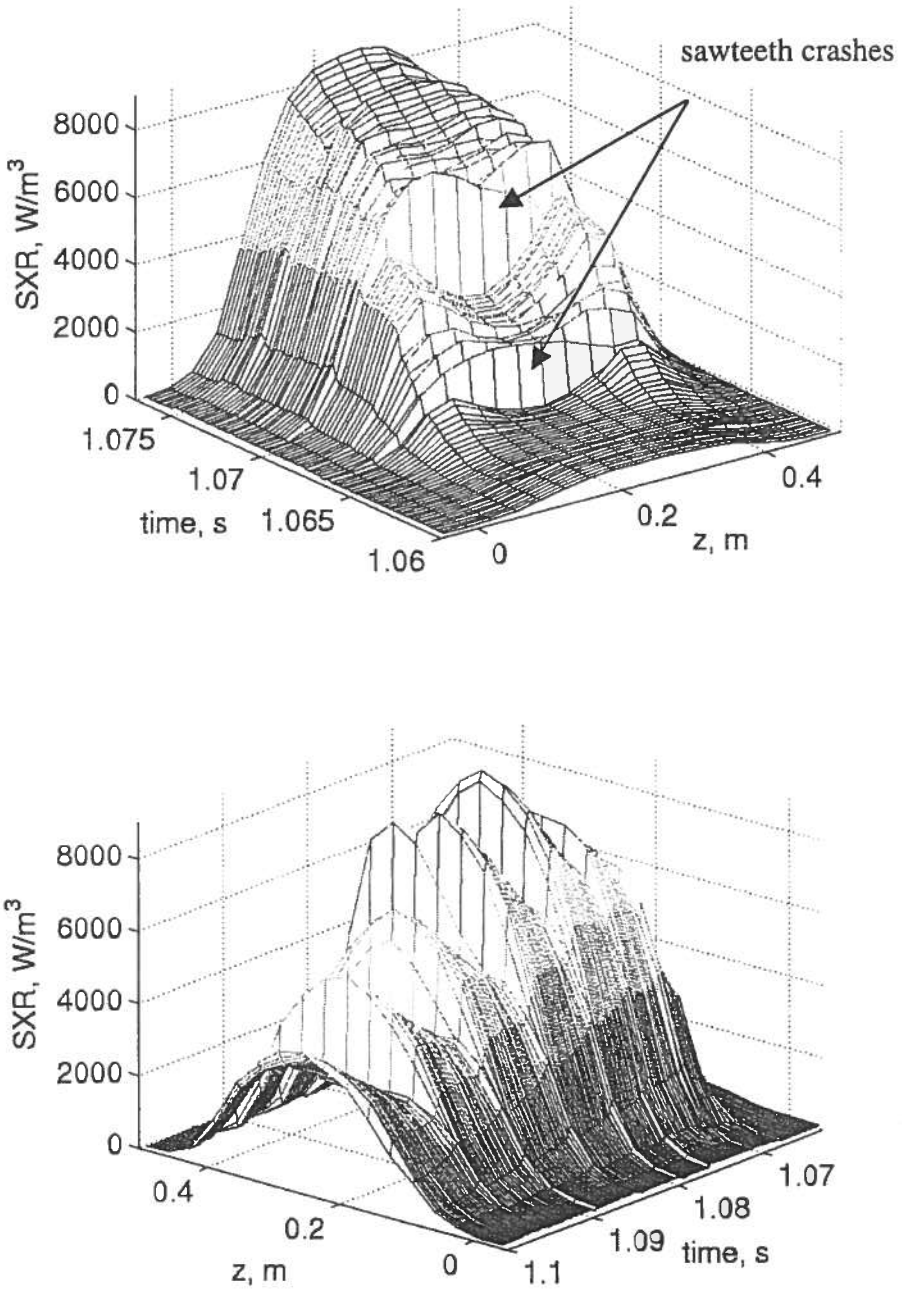

Figure 3 Tomographic reconstruction of the data from soft X-ray cameras for shot 16051. Top: ingress phase of the signal. Bottom: depletion phase

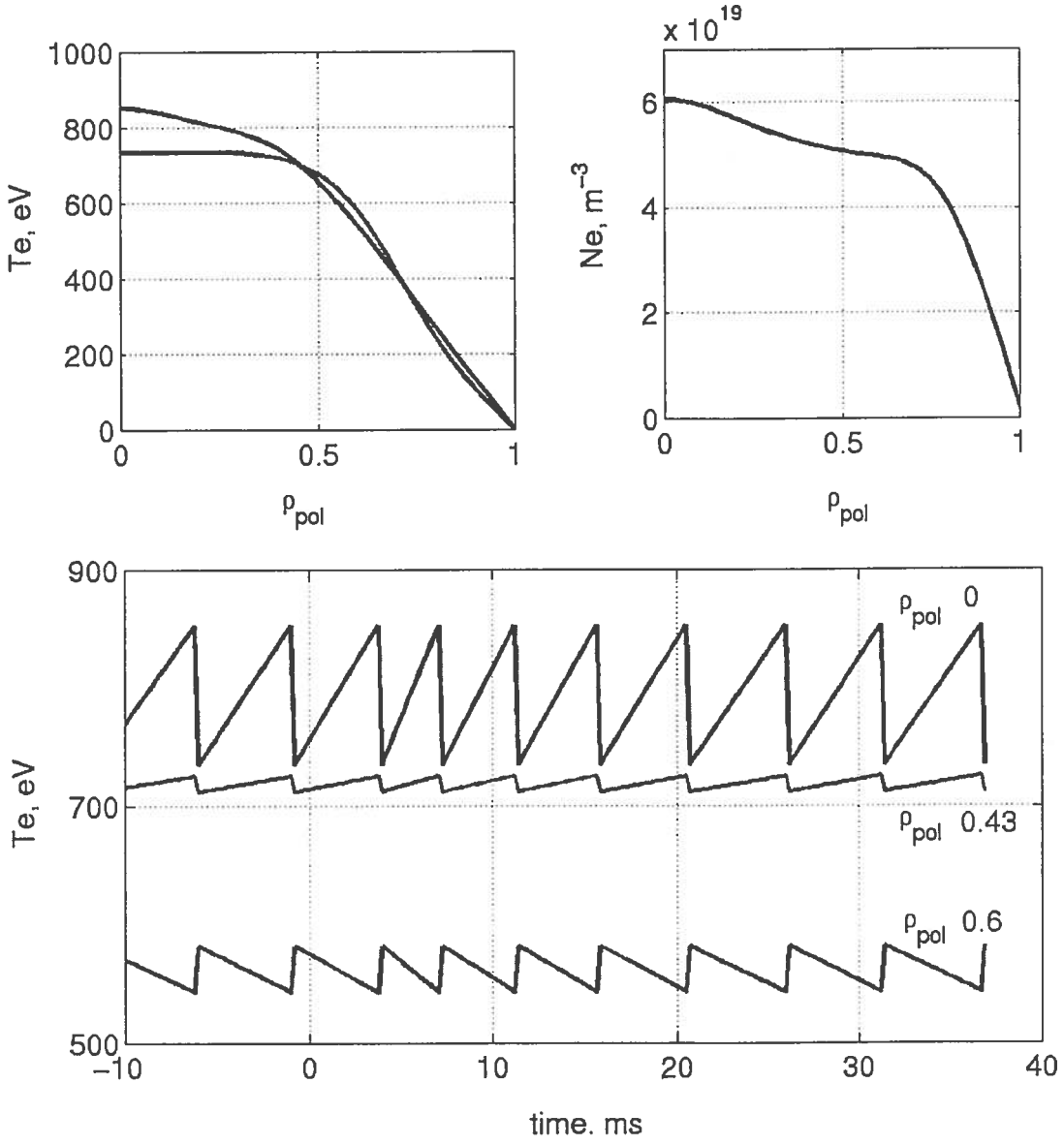

Figure 4 The electron density and the temperature profiles used for simulation of shot 16051.

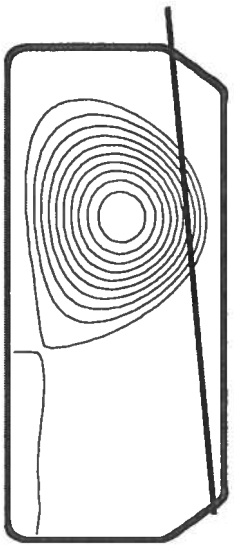

Figure 5 Location and viewing chord geometry of first channel of fast bolometric system. Plasma geometry of shot No. 16051

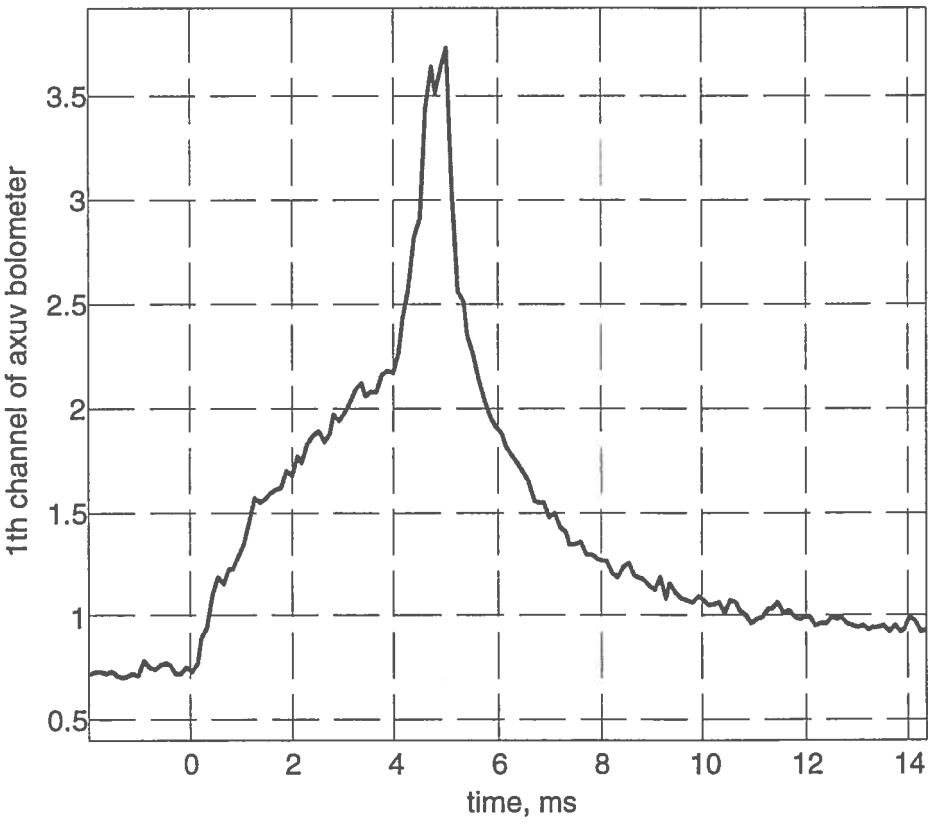

Figure 6 Signal of first channel of fast bolometric system. Zero time corresponds to the start of the injection.

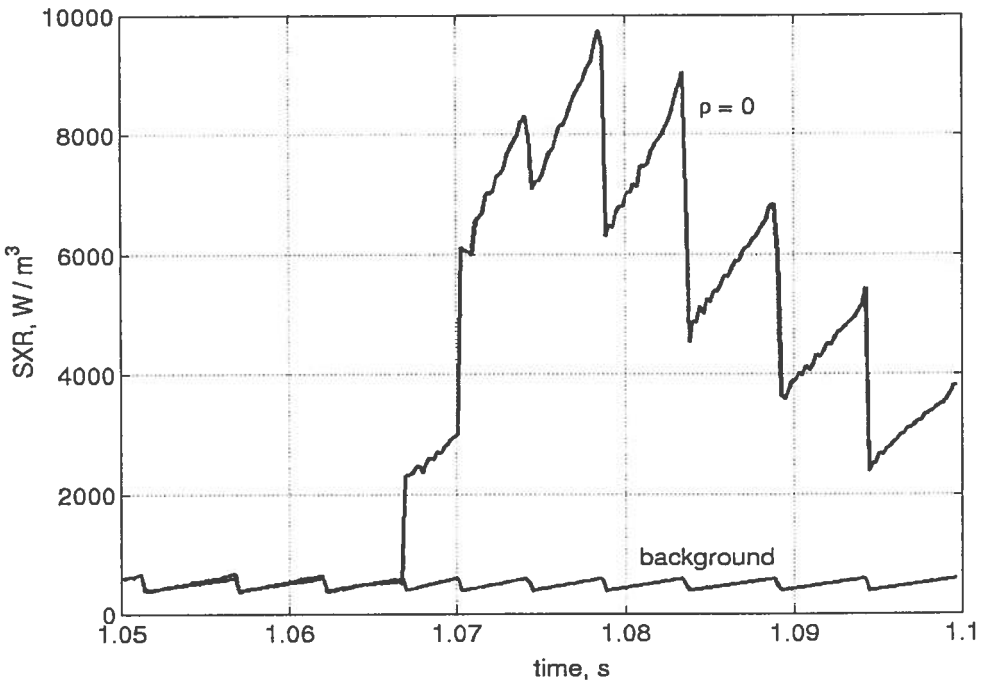

Figure 7 SXR emission followed to the injection and the background radiation for shot 16051

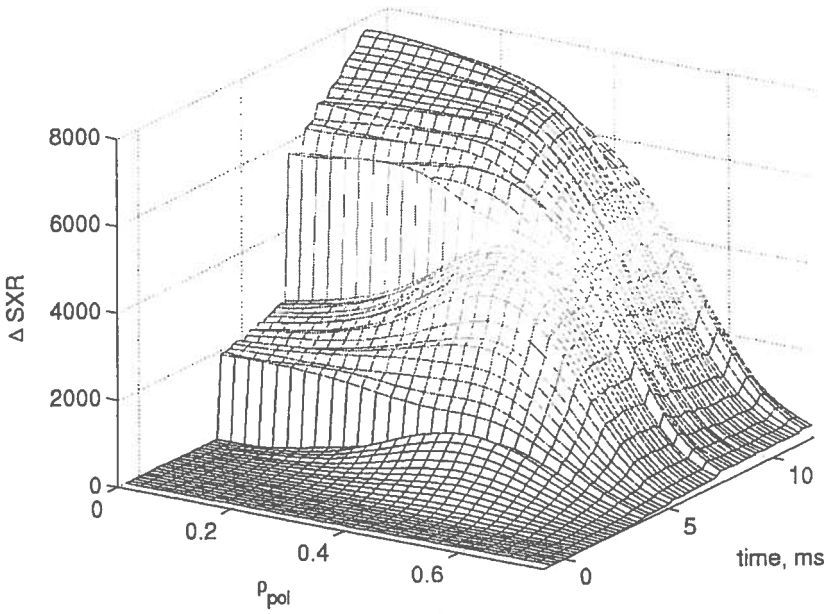

Figure 8 Reconstructed SXR profiles on standard ρ grid (normalised flux) after the subtraction of the background radiation. Ingress phase.

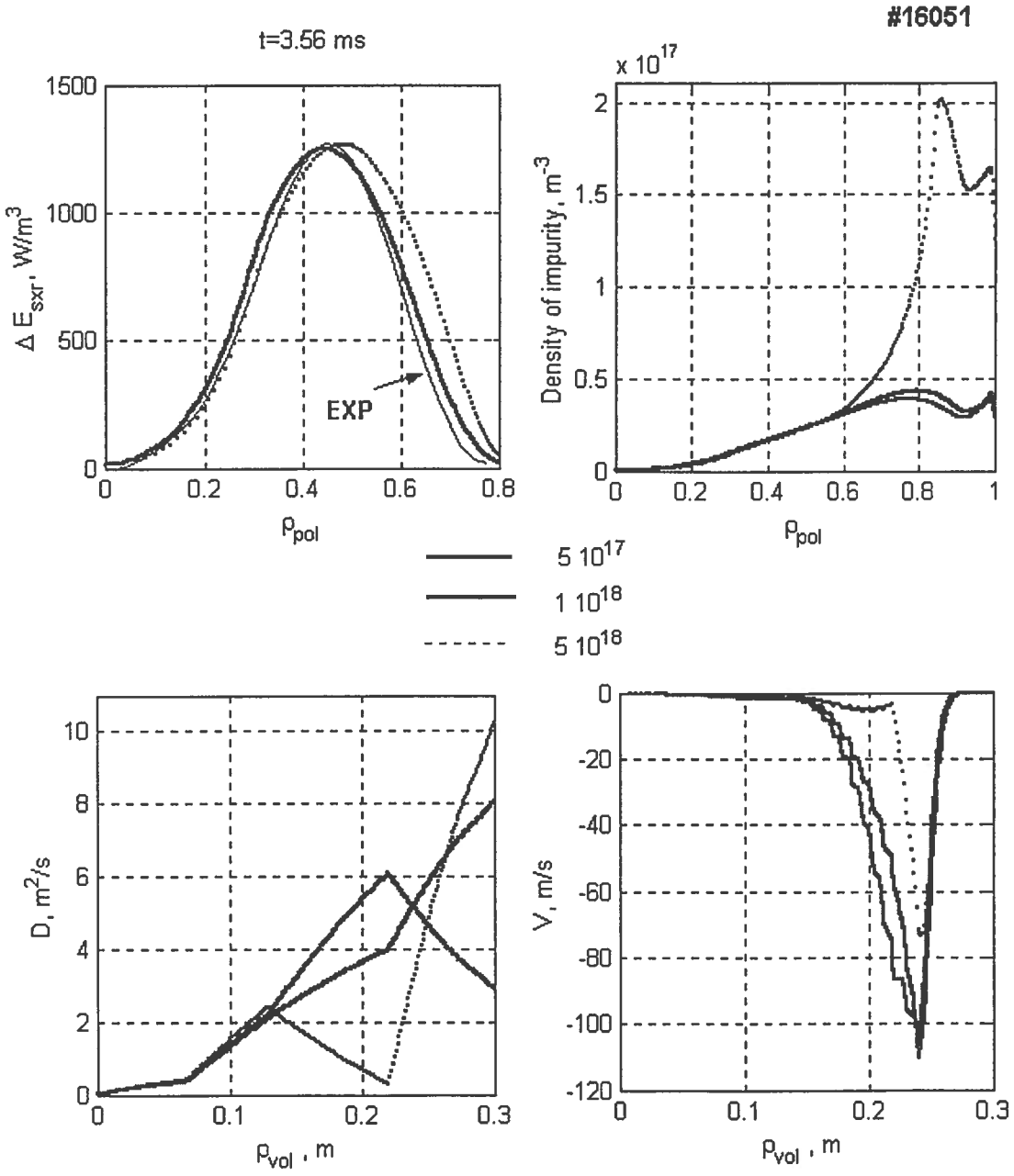

Figure 9 Example of fitting procedure for first quiescent phase with different normalisations of source function.

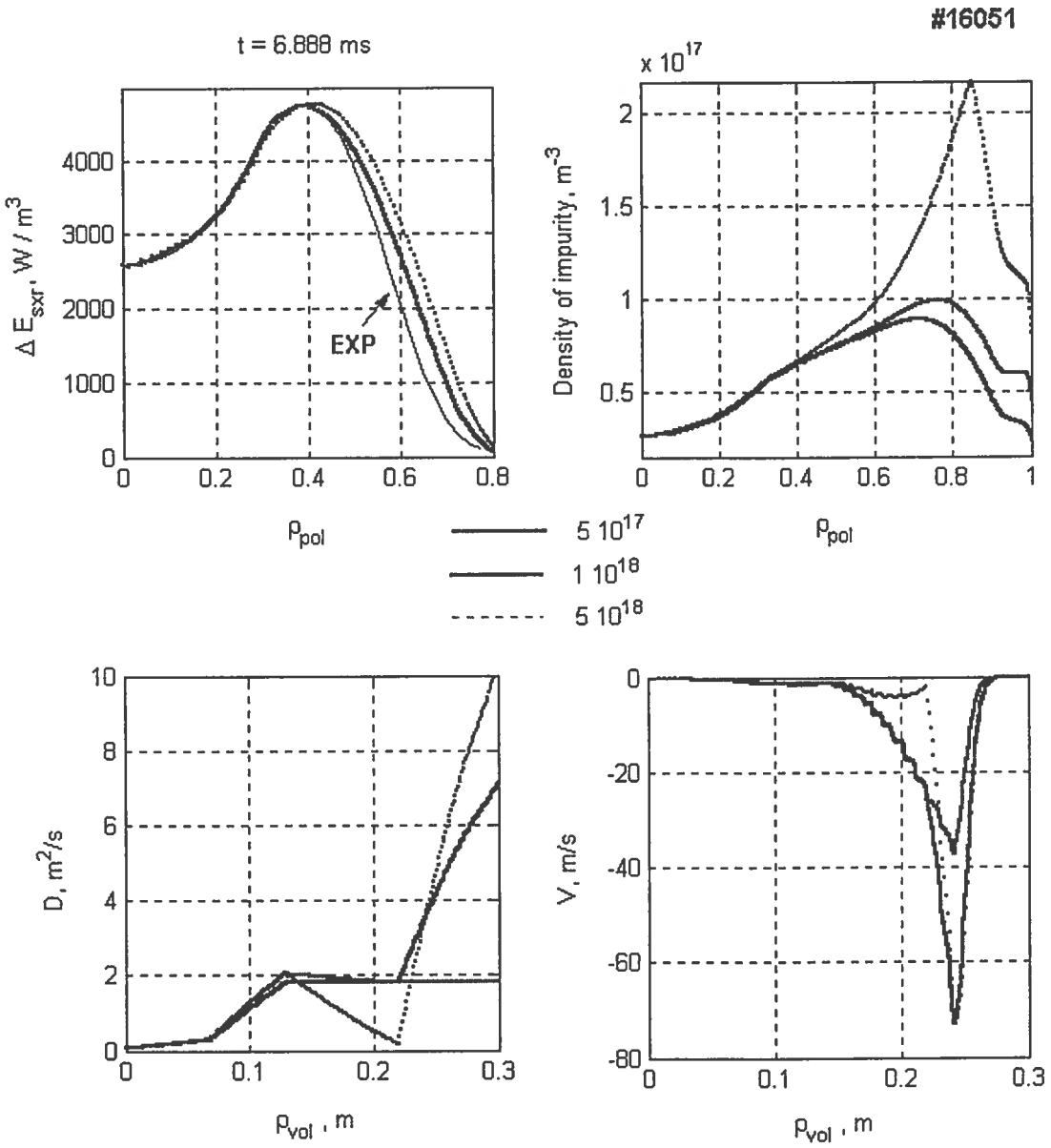

Figure 10 Example of fitting procedure for second quiescent phase with different normalisations of source function.

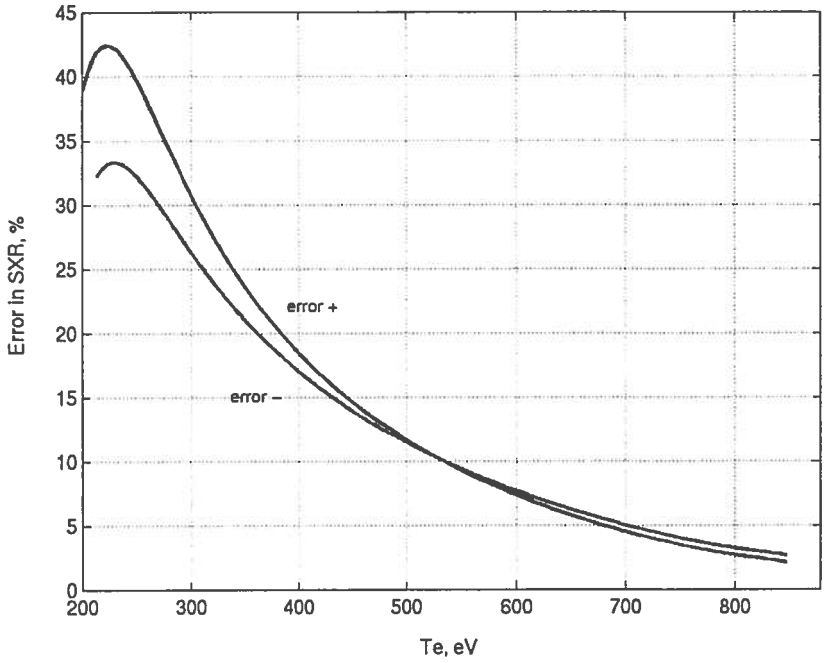

Figure 11 Influence of ±5 % errors in temperature on the simulated SXR (temperature dependence)

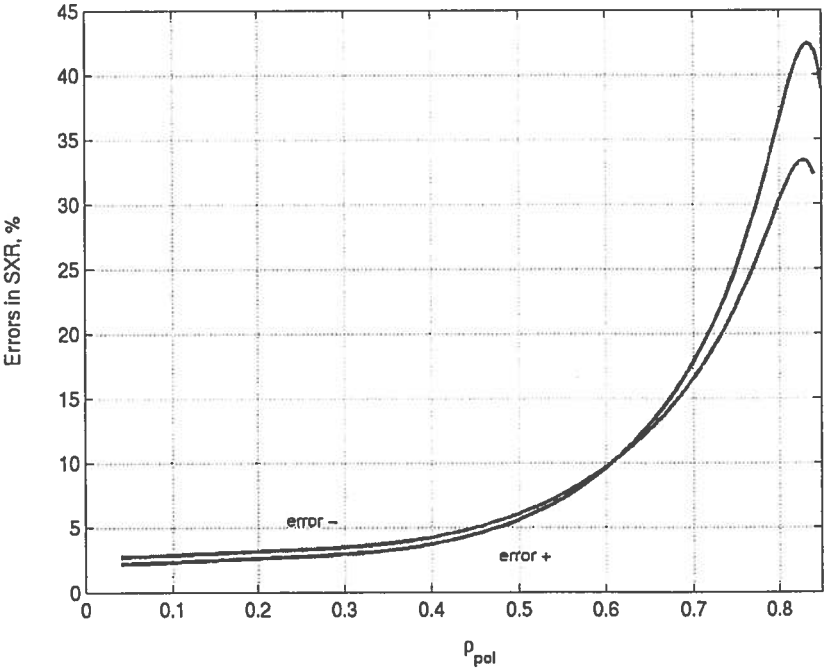

Figure 12 Influence of ±5 % errors in temperature on the simulated SX (radial dependence) for shot 16051.

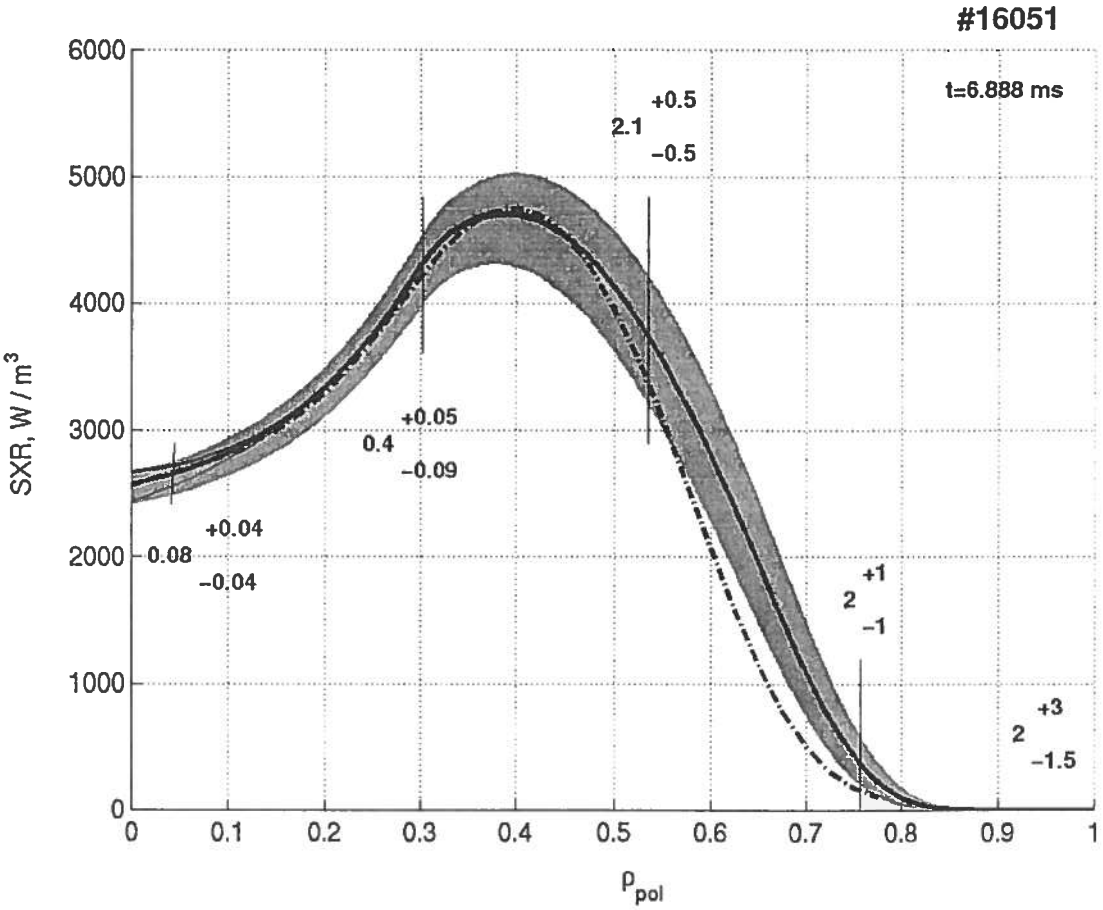

Figure 13 Influence of error in temperature on simulated profile of SXR. Filled area corresponds to errors in SXR due to errors ± 5 % in temperature. Solid line is STRAHL simulated SXR and dashed one comes from experiment. The thin lines near the centre correspond to the changes of central transport on 50 %. The thin vertical lines indicate the interpolation points.

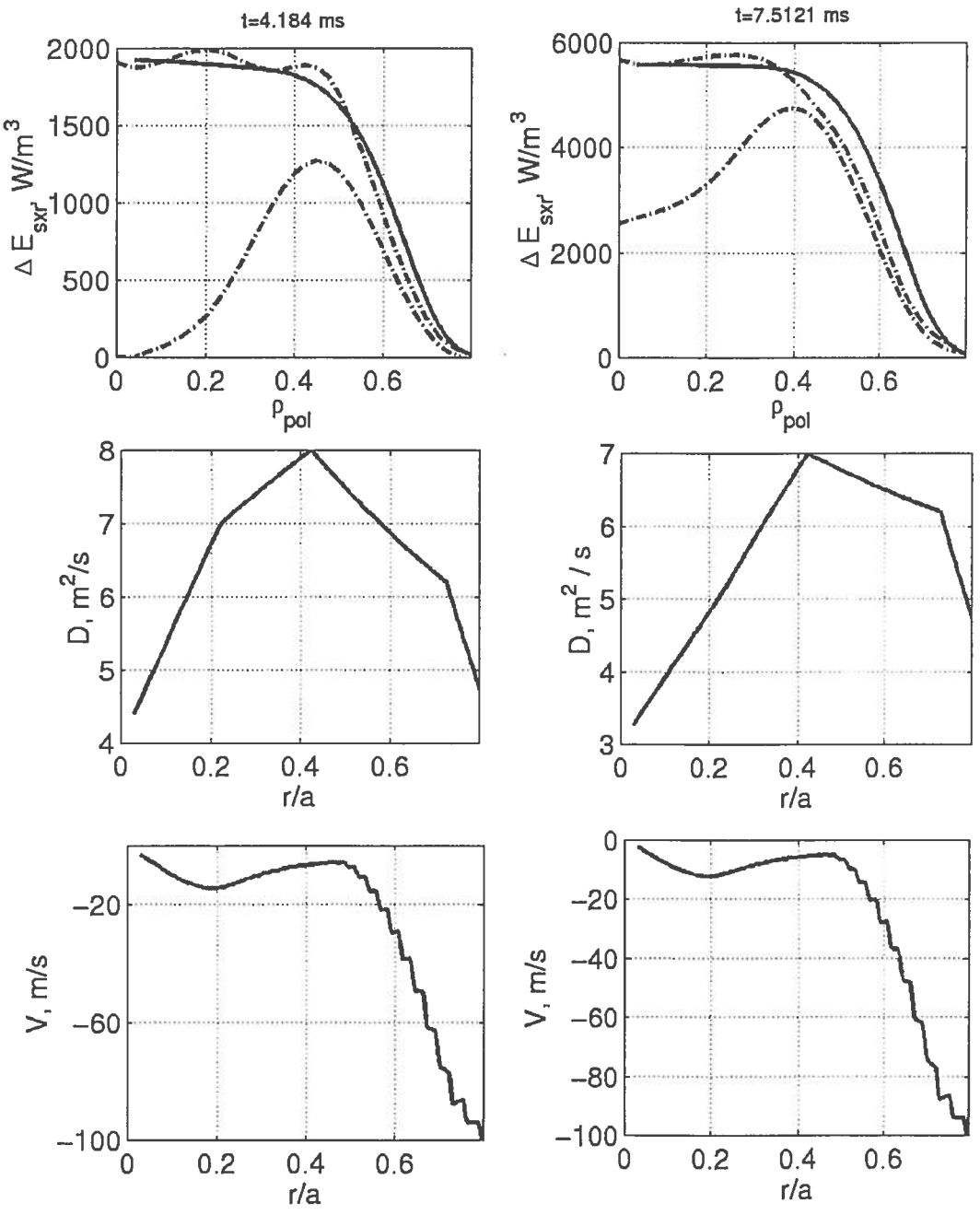

Figure 14 Example of the fitting procedure for first and second sawtooth crashes.

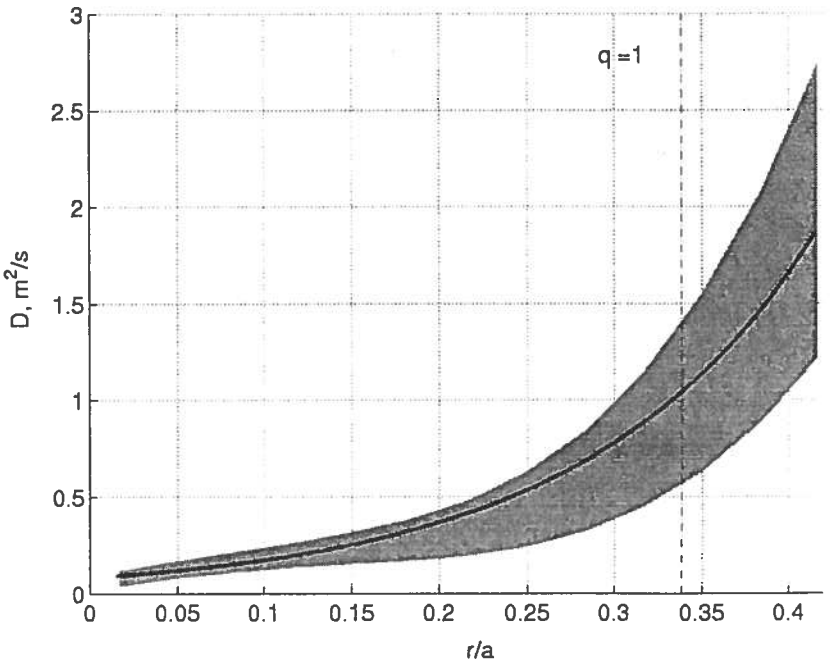

Figure 15 Diffusion coefficient for quiescent phases of shot 16051. Solid line represents an exponential approximation *D=0.08*exp(r/4)* where r is in cm.

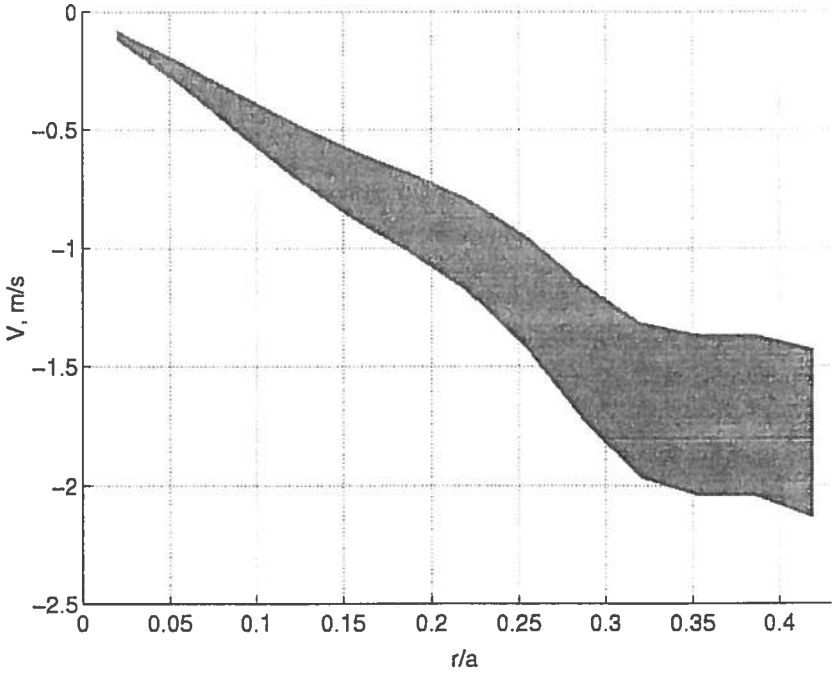

Figure 16 Drift velocity for quiescent phases of shot 16051.

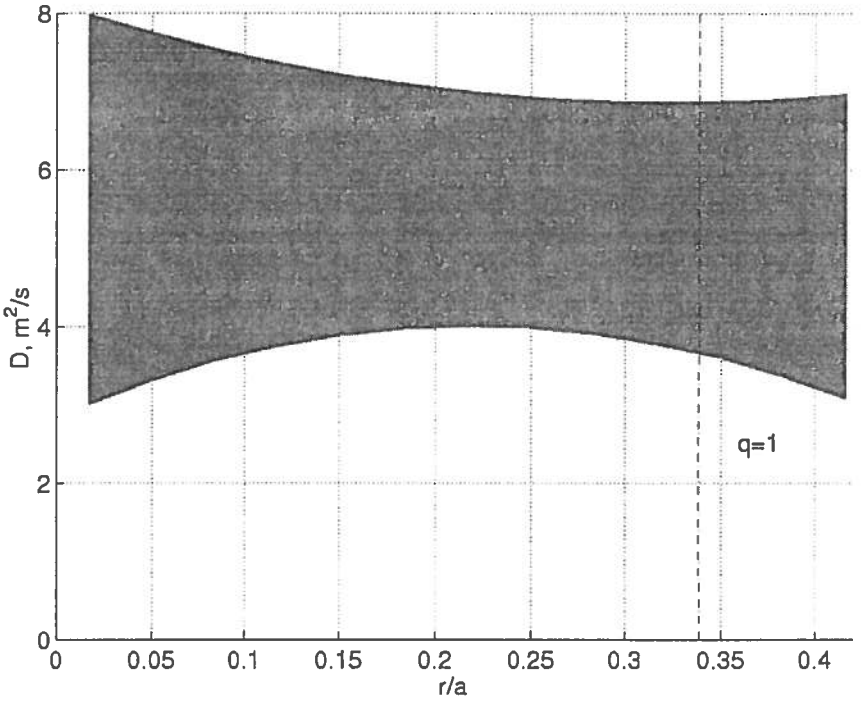

Figure 17 Diffusion coefficient for first crash phase of shot 16051

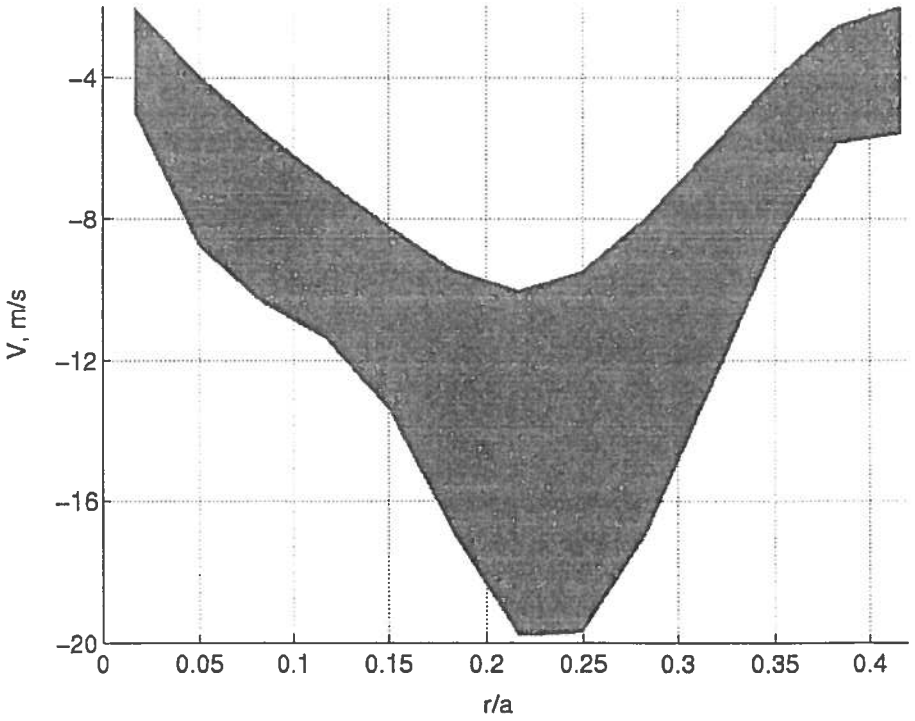

Figure 18 Drift velocity for first crash phase of shot 16051

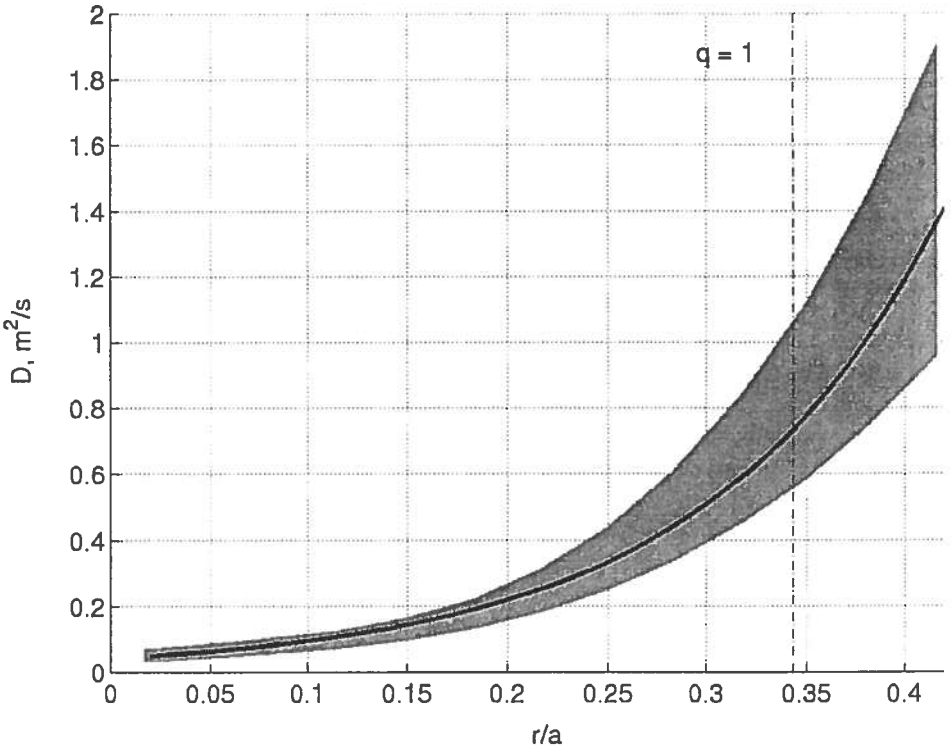

Figure 19 Diffusion coefficient for quiescent phase of shot 16079. Solid line represents an exponential approximation *D=0.04*exp(r/3.6)* where r is in cm.

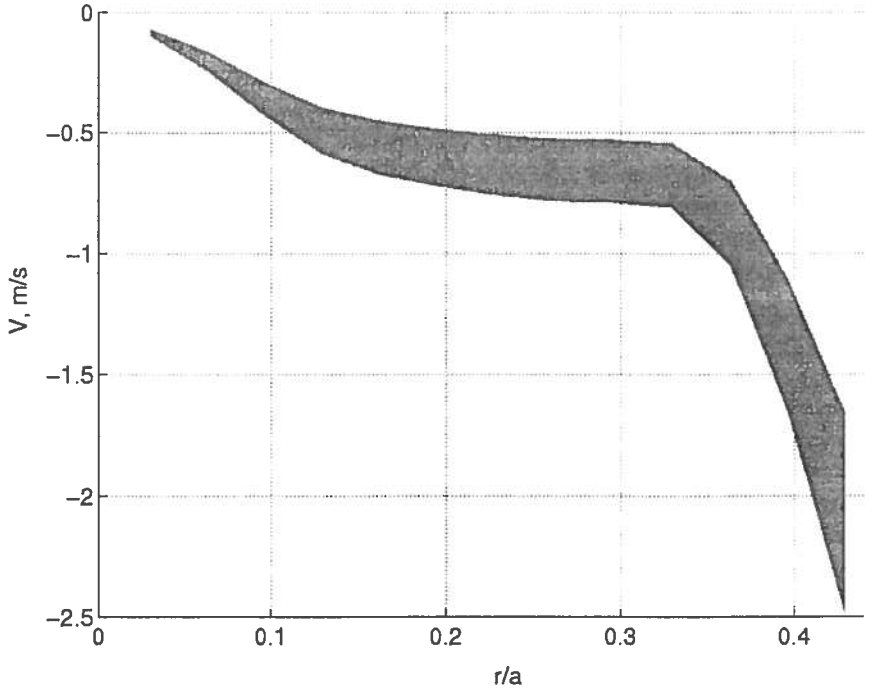

Figure 20 Drift velocity for quiescent phase of shot 16079

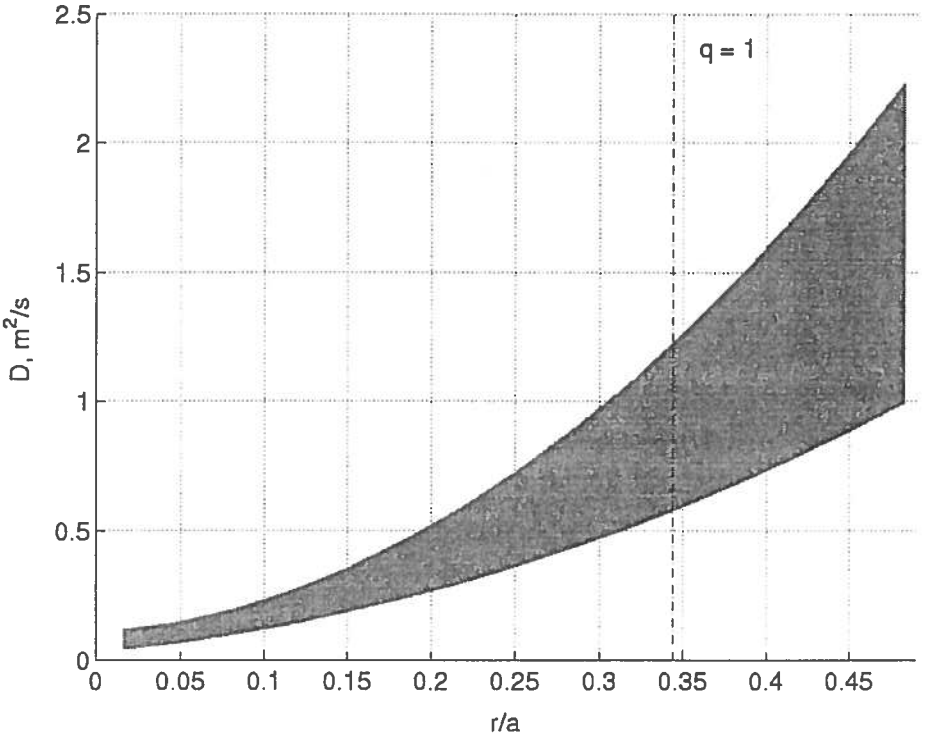

Figure 21 Diffusion coefficient for quiescent phases of shot 16574

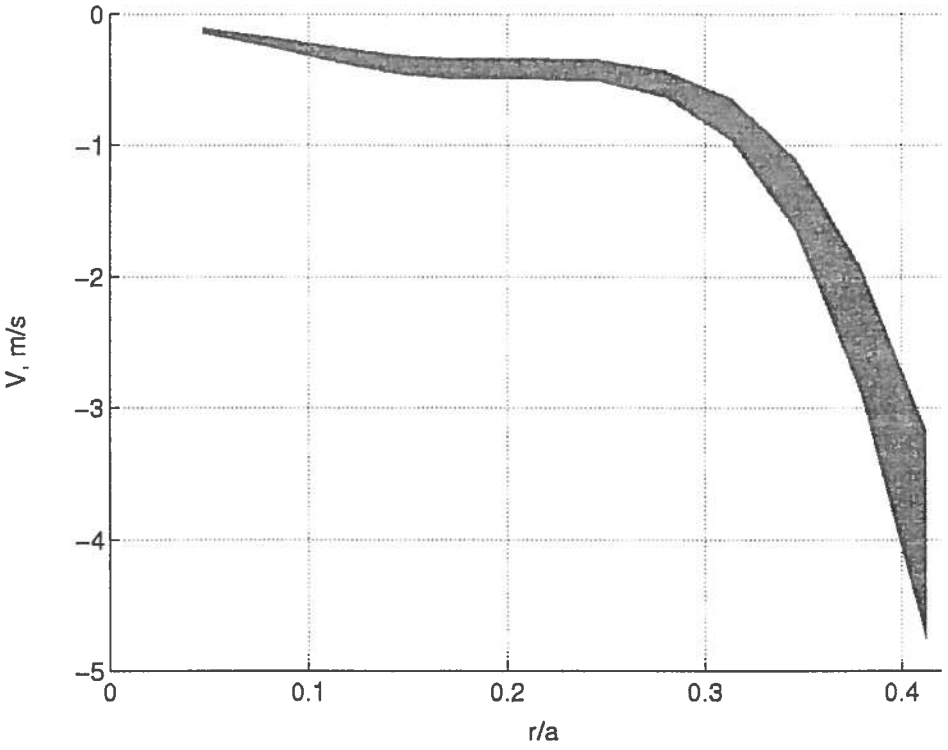

Figure 22 Drift velocity for quiescent phases of shot 16574

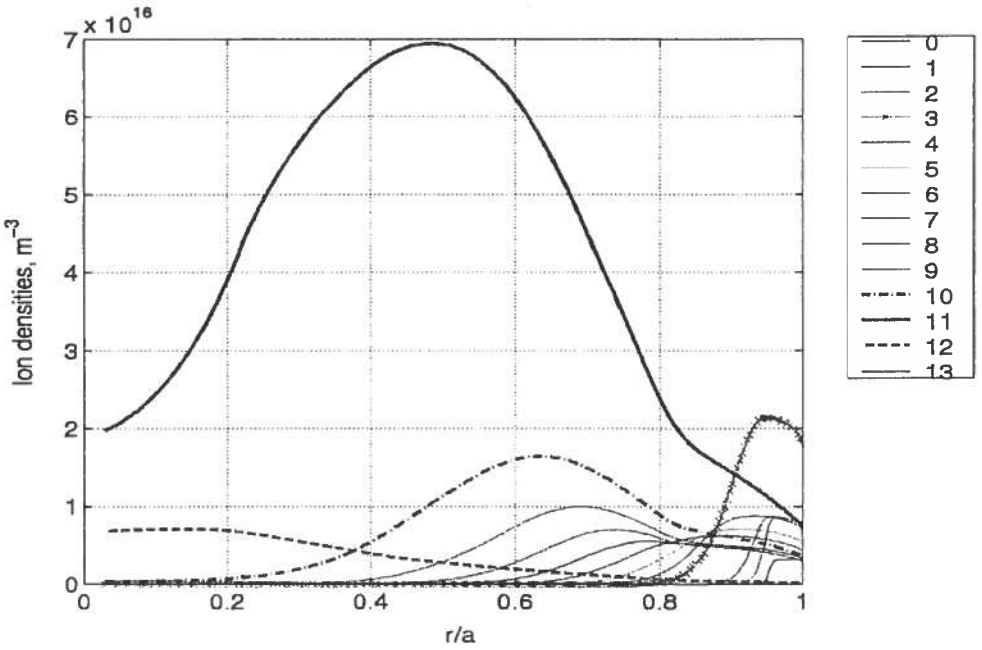

Figure 23 Ion densities for the end of second quiescent phase of shot 16051. Time=7 ms from the beginning of the injection

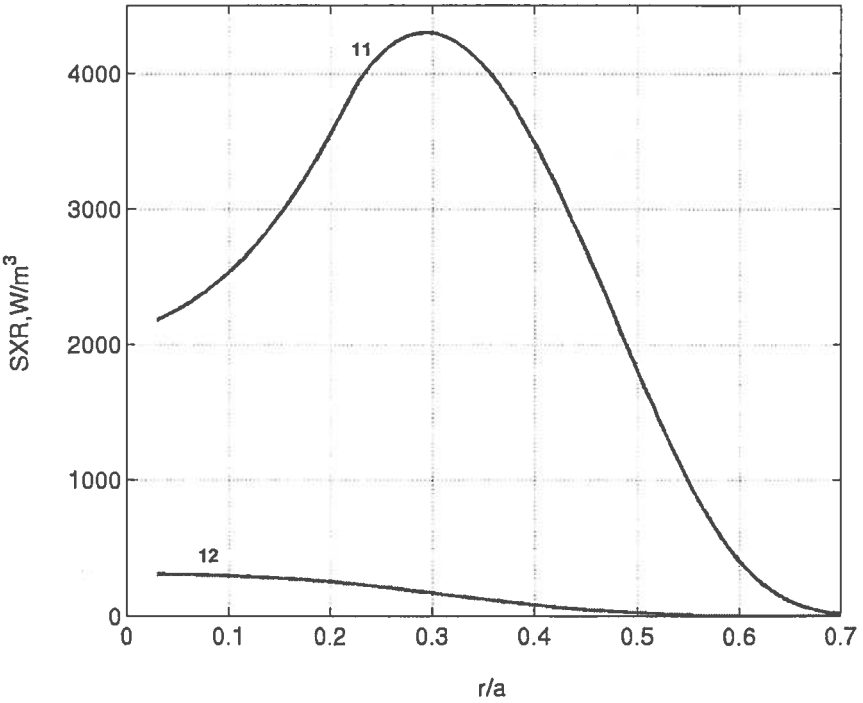

Figure 24 SXR from ionisation stages for ion distribution of previous figure

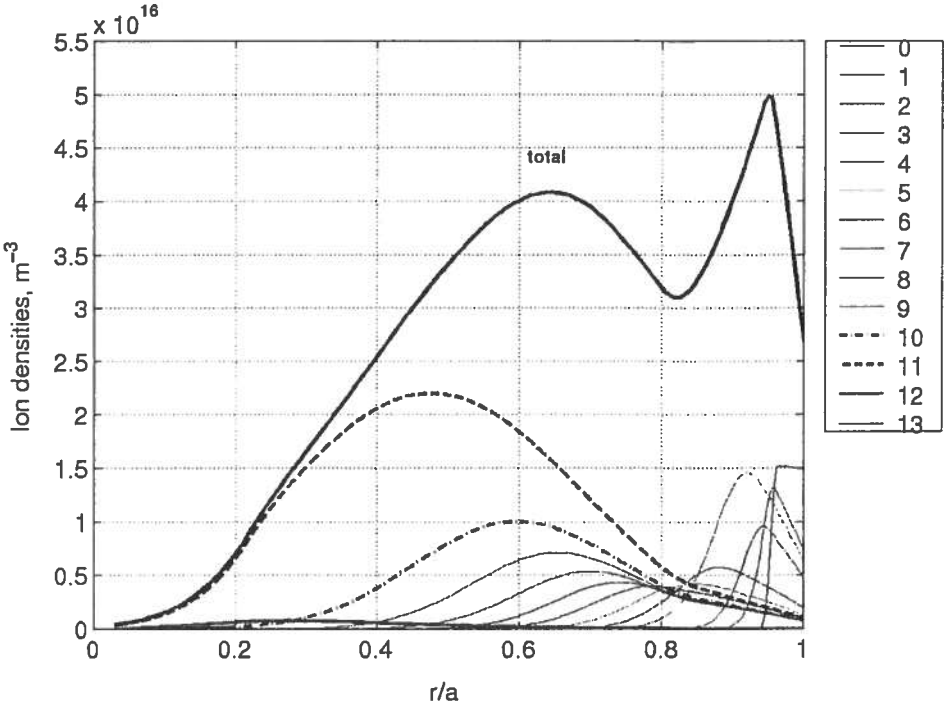

Figure 25 Ion densities just before first sawtooth crash for shot 16051 (3.8 ms from the beginning of the injection).

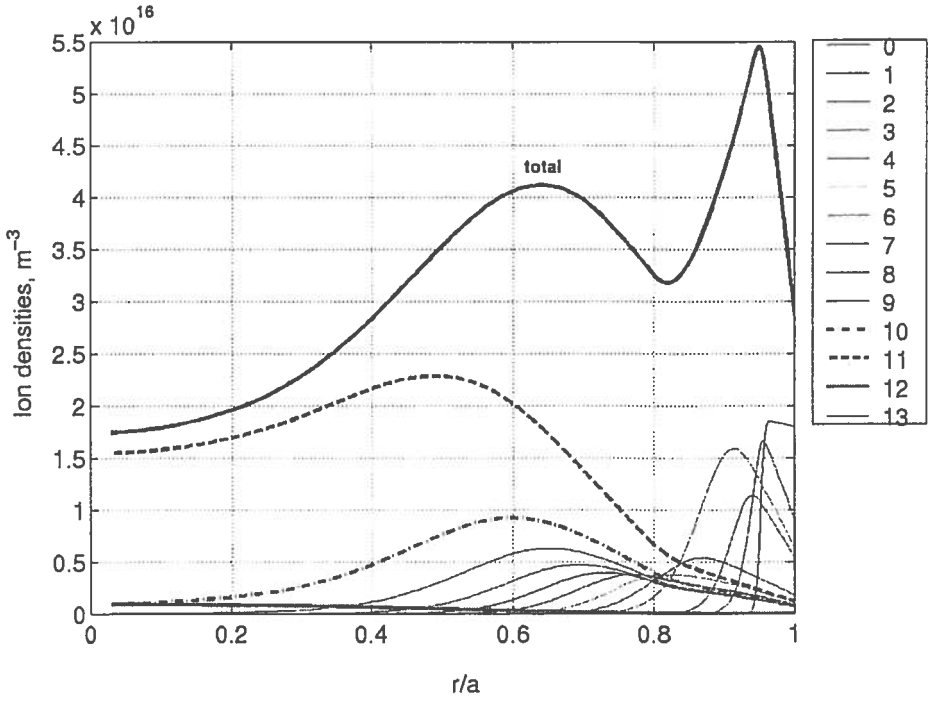

Figure 26 Ion densities just after first sawtooth crash for shot 16051 (4.1 ms from the beginning of the injection).

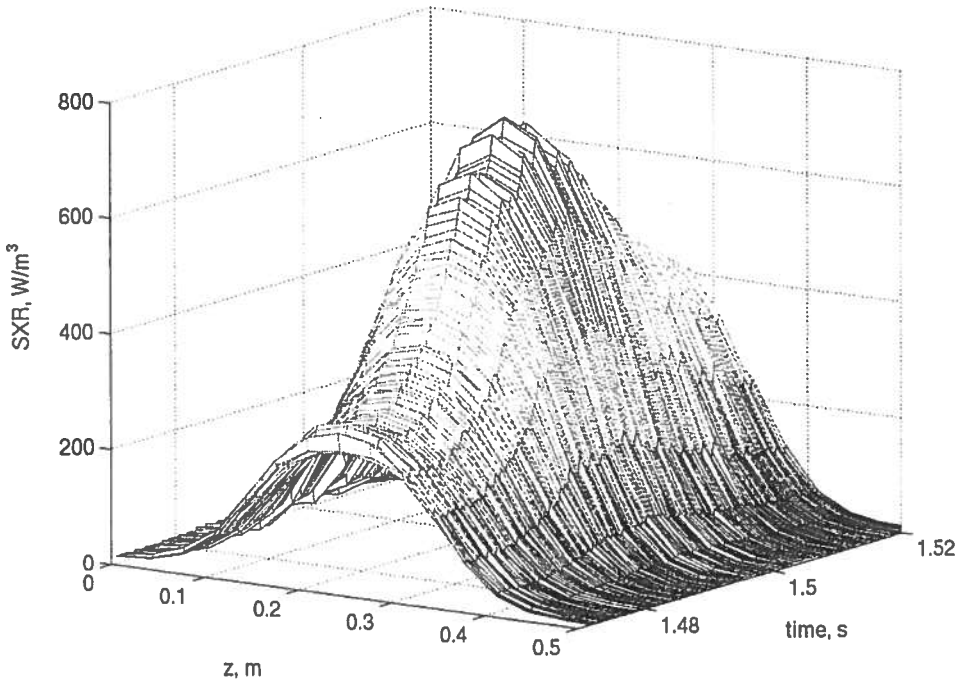

Figure 27 Tomographic reconstructions of SXR for shot 17747

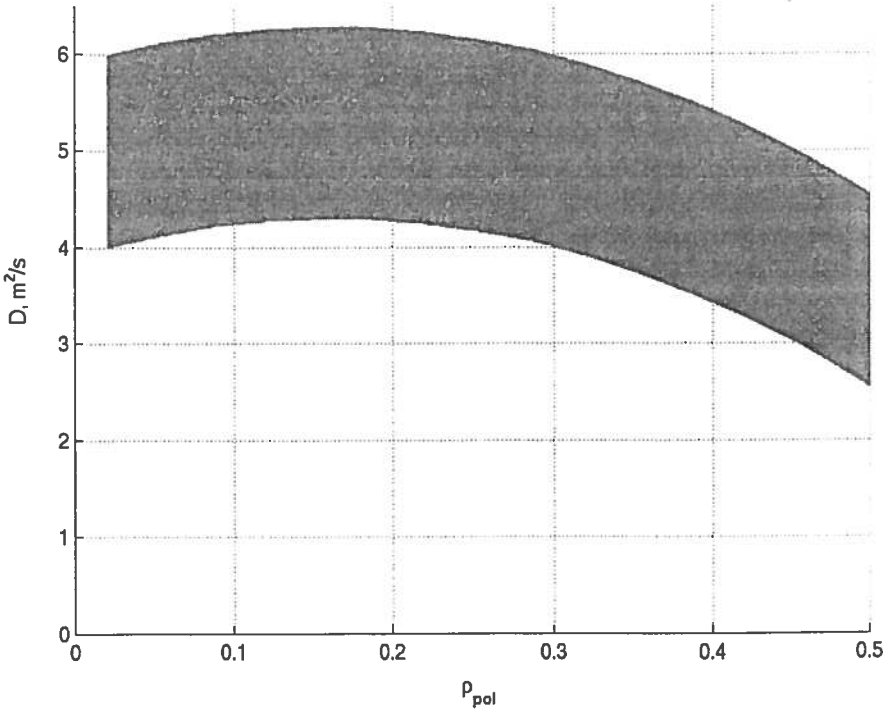

Figure 28 Effective diffusion coefficients for shot 17747